RSC Advances

PAPER

View Article Online
View Journal | View Issue

Cite this: *RSC Adv.*, 2021, **11**, 10272

A specific selenium-chelating peptide isolated from the protein hydrolysate of *Grifola frondosa*

Yu Xiong,†[a] Zi-Hong Chen,†[b] Feng-Li Zhang,[a] Zhi-Ying Yu,[a] Bin Liu, *[ab] Chong Zhang*[c] and Li-Na Zhao *[a]

Background: *Grifola frondosa* is a type of edible medicinal mushroom with abundant proteins. Selenium (Se) is an essential micronutrient for human. Many animal experiments and clinical studies had indicated that Se plays an important role in diverse physiologic actions. Most inorganic selenium compounds are toxic, and the lowest lethal dose is relatively small. Peptide-Se chelate can probably be dietary supplements in functional foods for humans with Se deficiency. *Methods*: In this study, a specific tripeptide Arg-Leu-Ala (RLA) with strong Se-chelating capacity was purified from *Grifola frondosa* through ultrafiltration, reversed-phase HPLC and gel filtration chromatography. The UV, SEM, XRD, ^{1}H NMR spectra are shown to provide more information about characterization of RLA-Se chelates. The bioavailability of RLA-Se chelate in Caco-2 cell line was investigated by using human colon cancer Caco-2 cells as model. iTRAQ comparative proteomics approach were used to identify the differentially expressed proteins. *Results*: The Se binding capacity of RLA was 84.47 ± 1.21 mg g^{-1}. The results of UV, X-ray diffraction (XRD), ^{1}H NMR and SEM structure analysis showed that the binding of selenium in the hydrolysate of *Grifola frondosa* protein was successful, and the amino and carboxyl groups of RLA were involved in the coordination of Se, which was the main site of chelation. The results of absorption of RLA-Se chelate in Caco-2 cells showed that RLA-Se chelate could be used as selenium supplement source. Using iTRAQ comparative proteomics approach, 40 proteins found significant. RLA-Se treatment had been demonstrated to present a higher accumulation of Se compared with control treatment and show an effective absorption by Caco-2 with the result that E3 protein performed up regulation. RLA-Se may play roles in cell cycle and apoptosis as an essential micronutrient. To sum up, our research results show that Grifola polypeptide-Se chelate is a promising multifunctional organic selenium product, which can be used as a new functional supplement for selenium deficiency.

Received 28th December 2020
Accepted 26th February 2021

DOI: 10.1039/d0ra10886c

rsc.li/rsc-advances

1 Introduction

Selenium (Se) is an essential trace element necessary for the normal development and maintenance of immune function in both humans and animals.[1] It has many physiological effects, such as anti-oxidant, anti-tumor, anti-bacterial, radioprotective, and immune-boosting properties.[2–4] Se deficiency is mainly due to environmental pollution, poor living habits, and aging. Se is a trace element required by the human body and about one billion people suffer from Se deficiency worldwide.[5] Se deficiency and homeostasis are related to many diseases and disorders, such as cardiovascular disease, infertility, gestational diabetes, and obstetric cholestasis.[6–8] The development of artificial selenium supplements has become a hotspot in nutrition research. However, most inorganic Se compounds are toxic, and the minimum lethal dose is relatively low.[9,10] Therefore, organic Se compounds with high biological activity, low toxicity, and few side effects are the desirable features of these supplements. Peptides with mineral-chelating abilities and other biologically active functions have been isolated from the proteolysis products of foods, such as proteins from chickpeas,[11] scallops,[12] shrimp,[13] sugarcane yeast,[14] and corn.[15] These peptides are capable of chelating minerals such as calcium,[16–18] zinc,[19] and iron and enhancing their bioavailability.[20] Nevertheless, the Se-chelating peptides in various proteins remain mostly unexplored.

Grifola frondosa (GF, *Basidiomycetes*, *Aphyllophorales*, *Polyporaceae*) is an edible, medicinal mushroom, known for its high levels of polysaccharides, steroids, phenols, and proteins. The protein content of *Grifola frondosa* is up to 35% per 100 g of the dry product, which is twice as much as that of shiitake mushrooms.[21] The biological components of *Grifola frondosa* have

[a]*National Engineering Research Center of JUNCAO Technology, Fujian Agriculture and Forestry University, No. 15, Shangxiadian rd, Cangshan District, Fuzhou, Fujian 350002, China. E-mail: liubin618@hotmail.com; zln20002000@163.com*

[b]*College of Food Science, Fujian Agriculture and Forestry University, Fuzhou, Fujian 350002, China*

[c]*Institute of Emergency Medicine, Department of Emergency, Fujian Provincial Hospital, Fuzhou, Fujian 350001, China. E-mail: czhang1@163.com*

† Co-first authors.

been shown to have antitumor,[22] immunity-enhancing,[23] antiviral,[24] and antioxidant activity.[25,26] Several studies have shown that the bioactive polypeptides obtained using proteolytic hydrolysis have better solubility, can be easily digested and absorbed, and have many unique physiological functions.[27] The whey polypeptide–ferrous chelate[28] and oyster–zinc chelate[29] showed better ion solubility than their corresponding inorganic salts in a simulated gastrointestinal digestion experiment. Using animal experiments, Chaud *et al.*[30] proved that the casein peptide–ferrous chelate has an effect similar to that of ferrous sulfate in the conversion rate of rat hemoglobin. By chelating covalent chemical bonds with metal ions, the cost of trace elements can be reduced, and the bioavailability of proteins and trace elements can be improved. Most studies have focused on the characterization of inorganic Se or the metabolic functions related to Se. The purification of Se-binding peptides extracted from GF protein hydrolysate (GFPH) has not been extensively explored. The rapid growth in various omics technologies over recent years has provided avenues and opportunities for selenium-related bioinformatics research.[31] Isobaric tags for relative and absolute quantitation (iTRAQ) labeling technology enables high-throughput screening of proteins, which is a useful approach in the interpretation of genomic information that facilitates the search for new therapeutic mechanisms.

In this study, a new chelating process was developed, wherein GFPH and Se were combined to form a new organic selenium supplement. The chelating mechanism was analyzed using ultraviolet spectroscopy (UV), scanning electron microscopy (SEM), X-ray diffraction (XRD), and ^{1}H-nuclear magnetic resonance (^{1}H-NMR). At the cellular level, the absorption properties of the novel organic selenium supplements were investigated, and the peptide fragments were identified using mass spectrometry. Lastly, proteomics data showed that our Se-chelating peptide had specific physiological effects.

2 Material and methods

2.1 Materials

GF was provided by Jingxiang Ecological Technology Industry Co., Ltd. Alkaline protease and Sephadex G-25 were purchased from Beijing Solarbio Technology Co., Ltd. All other chemicals and solvents were of analytical grade.

2.2 Preparation of GFPH

The GF powder was sieved through a #40 mesh, dissolved in deionized water to yield a concentration of 3% (w/v), and hydrolyzed using alkaline protease. The dosage of the enzyme was 5.0% (w/w, defined as enzyme mass/substrate mass × 100%) and the pH was adjusted to 10. The reaction was carried out in a constant temperature oscillator at 50 °C for 1 h.[32] The supernatant was centrifuged after cooling and stored at 4 °C until further analysis.

2.3 Purification of Se-binding peptides

2.3.1 Ultrafiltration. To isolate peptides with different molecular weights, the GFPH was ultrafiltered using 10 kDa and 3 kDa Pellicon XL ultrafiltration disk membranes (Millipore Co., USA), and the filtrates were concentrated and lyophilized. The Se-binding ability of each component was evaluated by measuring the selenium content. Components showing the strongest chelating ability were collected for subsequent separation. Se levels were determined using 3,3-diaminobenzidine colorimetry[33] and the following equation:

$$\text{Se}\ \left(\mu\text{g g}^{-1}\right) = \frac{pV}{mN} \quad (1)$$

where p represents the standard mass concentration equivalent to Se determined using the standard curve (μg mL^{-1}), V represents the sample volume obtained using toluene extraction (mL), m represents the mass of sample (g), and N represents the ratio of sample volume/total volume (%).

2.3.2 Gel filtration using Sephadex G-25 column. The sample with the strongest Se-chelating ability obtained using ultrafiltration was weighed (100 mg), dissolved in 5 mL deionized water, filtered through a 0.2 μm membrane, and applied to a pre-equilibrated Sephadex G-25 column (100 × 2.0 cm). The peristaltic pump was set to a speed of 0.3 mL min^{-1} and washed with deionized water. The absorbance was measured using a UV spectrophotometer at 214 nm. After determining the chelating ability of selenium, the most active fractions were mixed and lyophilized.

2.3.3 Reversed-phase high-performance liquid chromatography (RP-HPLC) using a C18 column. In this study, a C18 semi-preparative RP-HPLC column (Φ 250 × 10 mm; Phenomenex Inc., Torrance, CA, USA) was used. The lyophilized sample was dissolved in deionized water to yield a concentration of 50 mg mL^{-1}. The sample volume was 200 μL and the flow rate was set to 4.0 mL min^{-1}. Deionized water containing 0.05% TFA (solvent A) and acetonitrile with 0.05% TFA (solvent B) was used as the mobile phase. The detection wavelength was 214 nm. After determining the binding capacity of Se, the most active fractions were mixed, concentrated, and lyophilized.

2.3.4 Identification of peptides using liquid chromatography-electrospray ionization/mass spectrometry (LC-ESI/MS) and peptide synthesis. LC-ESI/MS (Delta Prep 4000, Waters Co., Milford, MA) was used to identify the molecular weight and amino acid sequence of the purified Se-chelating peptide in the range of 300–3000 m/z. The identified peptide was synthesized using the solid-phase method by Xinghao Medicine Limited (Wuhan, China). The synthetic peptides were purified using HPLC. A Gemini-NX 100A C18 column (Φ 250 × 4.6 mm) was used and 10 μL of the sample was injected. The flow rate was set to 1.0 mL min^{-1} and the detection wavelength was 220 nm. The molecular weights were determined using MS. The samples were freeze-dried and stored at −20 °C.

2.4 Synthesis of GFPH-Se chelate

To the GFPH solution, 0.5 M sodium selenite solution was added in a volume ratio of sodium selenite : polypeptide 4 : 6. The pH was adjusted to 9.0 and the reaction was performed at 50 °C for 1.5 h. After cooling, the sample was centrifuged at 3970g for 10 min. To the resulting supernatant, five volumes of 95% ethanol were added and mixed well, and the chelate was

allowed to sediment for 12 h. Then, the sample was re-centrifuged at 5000 rpm for 10 min. The precipitated sediment at the bottom was collected and washed several times with anhydrous ethanol. The Se content of the GFPH-Se chelate was determined after freeze-drying using eqn (1).

2.5 Characterization of the RLA-Se chelates

2.5.1 Ultraviolet (UV) spectroscopy. RLA, sodium selenite and RLA-Se chelate samples were prepared at a concentration of 0.2 mg mL^{-1}, the pH was adjusted to 7.0, and their UV absorption spectra were obtained at a wavelength of 200–800 nm using a Spectra Mr instrument (Persee, Beijing) as previously described.[34] Each sample was analyzed in triplicate.

2.5.2 Scanning electron microscopy (SEM). Samples were sputter coated using gold and the morphologies of RLA and RLA-Se chelates were characterized using SEM (FEI, USA) under 1000× and 5000× magnification using the high vacuum mode. Samples of RLA and RLA-Se chelates were bonded to the sample table using a conductive adhesive. After the gold-plated treatment, the morphologies of RLA and RLA-Se chelates were characterized using SEM (FEI, USA) under 1000 and 5000 high vacuum conditions.

2.5.3 X-ray diffraction (XRD). The samples of RLA and RLA-Se chelates were analyzed using X-ray diffraction (Philips, Netherlands) using a scanning speed of 4° min^{-1} ranging from 5–75°, with a stepwise increment of 1°, and an emission slit 0.3 mm.

2.5.4 ^{1}H-NMR spectroscopy. RLA and RLA-Se chelate (about 0.5 mg each) were dissolved in 500 μL Milli-Q water; 500 μL tritium water was added and the sample was transferred to a 5 mm NMR (Bruker, Switzerland) test tube to obtain the ^{1}H-NMR spectra at 600 MHz.

2.6 The effect of RLA-Se chelate on the cellular uptake of Se

2.6.1 Cell culture. The human colon adenocarcinoma cell line, Caco-2, was obtained from the Institute of Bioengineering, Fuzhou University, and passed for 20–40 generations. DMEM supplemented with 20% fetal bovine serum and 1% double-antibody were used as cell culture media and the cells were cultured in an incubator at 37 °C in an atmosphere of 5% carbon dioxide. Cells were subcultured with 0.25% trypsin–EDTA at a ratio of 1 : 3.

2.6.2 Cytotoxicity test. The MTT assay with slight modifications[35] was used for cytotoxicity determination. The MTT assay reflects cell viability by detecting the activity of succinate dehydrogenase in the mitochondria of live cells. Caco-2 cells were seeded in a 96-well-plate at a density of 1×10^4 cells per cm^{-2} and incubated at 37 °C with 5% CO_2 for 24 h, after which, the medium was removed. DMEM (150 μL) containing 2, 4, 6, 8, and 10 μmol L^{-1} RLA-Se chelates and sodium selenite were added to each well of the treatment group. After incubation for 24 h, the solution was aspirated and 20 μL PBS solution containing 5 mg mL^{-1} MTT was added. After 4 h of incubation, MTT was removed and 150 μL dimethyl sulfoxide (DMSO) was added to each well to dissolve the purple formazan crystals. The OD of each well was measured using enzyme-linked immunosorbent assay (ELISA) at 560 nm. The results are expressed as a ratio to the control.

2.6.3 Cellular uptake studies. Caco-2 cells were incubated with different concentrations of the RLA-Se chelate and sodium selenite at 37 °C in a 5% CO_2 environment for one hour. Next, the cells were washed with PBS three times. Then, the cells were incubated with 1 mL of cell lysis buffer for 30 min on ice, transferred into 1.5 mL Eppendorf tubes, centrifuged at 4 °C for 5 min, and the supernatant was collected. The total protein concentration and Se content were determined using a published method described by Chen.[36] The results are expressed in μg mg^{-1} protein.

2.7 Proteomics of Caco-2 cells detected using iTRAQ

2.7.1 Protein extraction, digestion, and iTRAQ labeling. The following protocol was used to extract the total protein from the Caco-2 cell samples (control) and RLA-Se chelate-injected cell samples (treated). The cell samples were boiled in SDT buffer (8 M Urea, 100 mM Tris–HCl, 1 mM PMSF, 0.1 M DTT, pH 7.6) for 5 min and homogenized using FastPrep-24 (MP Biomedicals, 6M/S, 30 s, two cycles), treated using ultrasound (100 w, 30 s on, 30 s off, 10 cycles) and centrifuged. Protein levels were quantified using the Bradford method.[37] Protein digestion was performed according to the FASP procedure described by Wisniewski, Zougman *et al.*[38] The resulting peptide mixture was then labeled with 8-plex iTRAQ reagent following the manufacturer's instructions (Applied Biosystems). The samples were labeled as Treated (M, N, and O) and Control (P, Q, and R), and were subjected to multiple treatments and vacuum drying.

2.7.2 Two-dimensional LC-MS/MS analysis using Q exactive. The peptide mixture (1 μL) was added to the C18 reversed-phase column (Thermo Scientific Easy Column, 15 cm long, 75 μm internal diameter, 3 μm resin) in buffer A (0.1% formic acid in water) and buffer B (0.1% formic acid in acetonitrile). The linear gradient was separated at a flow rate of 400 nL min^{-1}. Mass spectrometry data uses the top 20 methods associated with the data to dynamically select the most abundant precursor ions from the measurement scan (300–1500 m/z) of HCD fragmentation. The determination of the target value was based on predictive Automatic Gain Control (pAGC). The duration of the dynamic exclusion was 30 s. Survey scans were acquired at a resolution of 70 000 at m/z 200, and resolution for HCD spectra was set to 17 500 at m/z 200. The normalized collision energy was 27 eV. The instrument was operated with the peptide recognition mode enabled.

2.7.3 Bioinformatics analysis. The original data were collected and processed using the international mainstream proteomics analysis software, Proteome Discoverer 2.1, and a human database downloaded from the UniProt website (9606 sequences) was used. The differential proteins identified in this study were screened using differential multiple >1.2 or ≤0.83 and P-value ≤0.05. Using the bioinformatics analysis tool, David on-line analysis, GO (gene ontology) function annotation, location analysis, and function enrichment analysis were carried out for the identified proteins.

2.8 Statistical analysis

All results are expressed as means ± standard deviations (SD) of three experiments. Statistical analyses were performed using Student's t-test. A value of $P < 0.05$ was considered statistically

Table 1 Se-Chelating ability of peptides with different molecular weights

Fraction	Molecular size	Se-Chelating ability (mg g^{-1})
F1	<3 kDa	55.61 ± 4.16[a]
F2	3–10 kDa	21.99 ± 1.93[a]
F3	>10 kDa	38.74 ± 4.03[a]
GFPH	Untreated	23.50 ± 3.43[a]

[a] Significant difference was evaluated by Duan's *t*-test ($p < 0.01$), and data with the same letter are not significantly different ($p > 005$). All the samples were determined three times, and the results were reported as means ± SD.

significant, while a value of $P < 0.01$ suggested extremely statistically significant.

3 Results

3.1 Purification of Se-chelating peptide

The Se-chelating peptides with a molecular weight lower than 3 kDa were extracted from the enzymatic hydrolysate of the GF protein using ultrafiltration. Three peptides with different molecular weights were identified after ultrafiltration and their chelating abilities are shown in Table 1. Sephadex G-25 gel filtration chromatography was used to separate the component with the highest Se binding ability, which was named F1. Three components were separated, namely, F11, F12, and F13 (Fig. 1A). The chelating capacity of F12 was the highest (Fig. 1B). The eluent corresponding to the peak of F12 was collected and separated using semi-preparative C18 RP-HPLC. Fraction F12 was divided into 29 different main fractions (Fig. 2A). The peptide was dissociated using a 0.05% TFA-acetonitrile system. The high-signal fractions (1, 5, 13, 17, 22) were separated and lyophilized for LC-MS analysis.

3.2 Identification of peptides using LC-ESI/MS

For peptide identification, the high-signal fractions (1, 5, 13, 17, 22) were subjected to LC-MSD Trap Mass Spectrometry. The five peptides were sequence as Ser-Leu (SL), Thr-Leu (TL), Val-Leu (VL), Arg-Leu-Ala (RLA) and Met-Leu (ML), and its characteristic information is shown in Table 2. MS/MS spectra of RLA with m/z is shown in Fig. 2B. These sequences matched well with those stored in the National Center for Biotechnology Information (NCBI) database. The results showed that the Se-chelating peptides in GF contained 2–3 residues. However, no polypeptides were detected in fractions 1 and 5.

Table 2 Sequences of Se-chelating peptides identified from GFPH

No.	MW[a]	Sequence	Fraction	Abbreviation
1	219	Ser-Leu	13	SL
2	233	Thr-Leu	17	TL
3	231	Val-Leu	17	VL
4	359	Arg-Leu-Ala	17	RLA
5	263	Met-Leu	22	ML

[a] Molecular weight.

3.3 Se-Chelating ability of peptides

To ascertain whether the purified peptide had appreciable Se-binding ability, the Se-binding activities of the five peptides were determined (Fig. 2C). All peptides were found to be potential Se-chelating peptides. The highest Se-chelating ability of RLA was determined to be 84.47 ± 1.21 mg g^{-1}, which was significantly higher than that of TL (67.83 ± 1.49 mg g^{-1}) and ML (67.96 ± 3.35 mg g^{-1}).

3.4 Structural characterization

3.4.1 UV spectroscopy. It can be seen from Fig. 3 that the characteristic absorption peak of the tripeptide, RLA, is near 269 nm, which is caused by the chromogenic moieties such as the carbonyl and carboxyl groups and the amide bond. After chelating with Se, the characteristic absorption peak shifted to 275 nm, resulting in the redshift phenomenon. It is speculated that during the process of chelation, n → π* energy level

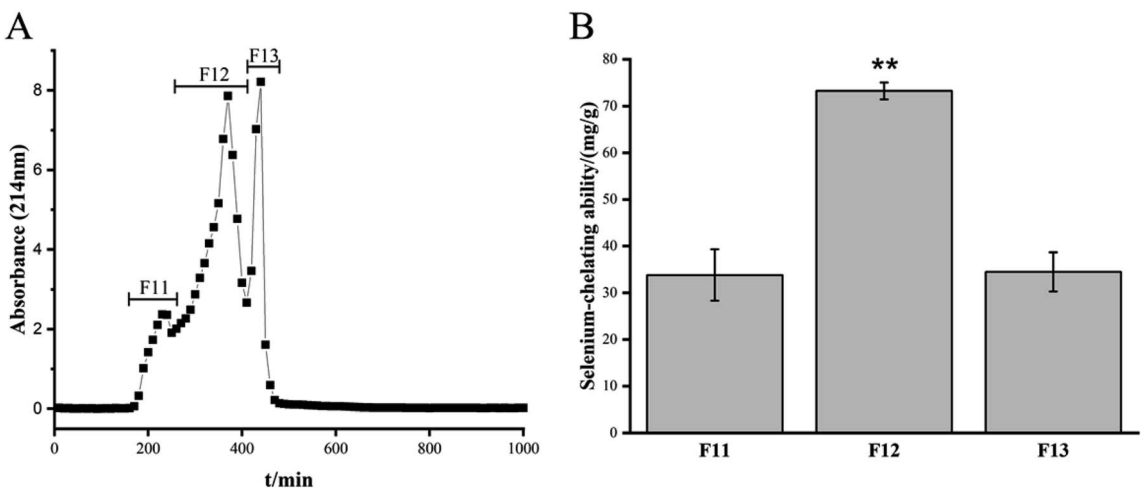

Fig. 1 Sephadex G-25 gel filtration chromatography from ultrafiltration and Se-chelating ability of the fractions from Sephadex G-25 column.

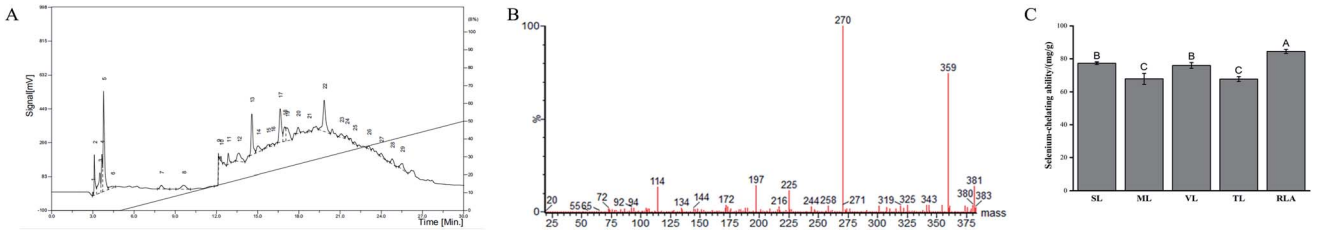

Fig. 2 Purification and identification of the Se-chelating peptide using semi-preparative C18 RP-HPLC and LC-ESI/MS. (A) Semi-preparative C18 RP-HPLC of fraction F12. (B) The mass spectrum of the RLA. (C) Se-Chelating ability of synthetic peptides. (A)–(C) Significant difference was evaluated by Duncan's multiple range test ($p < 0.01$), and data with the same letter are not significantly different ($p > 0.05$).

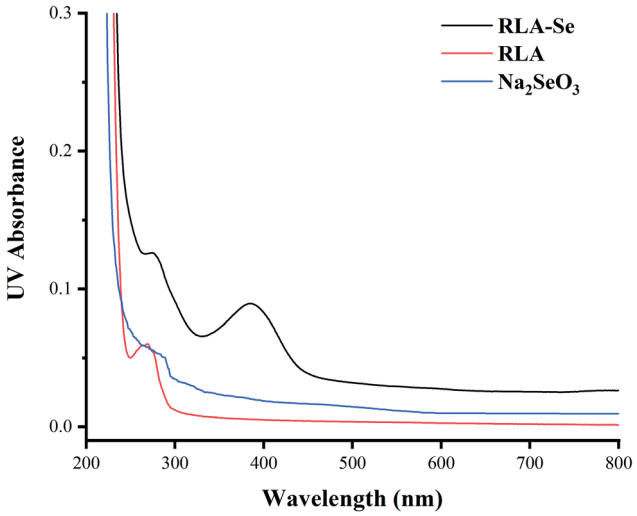

Fig. 3 UV spectrum of RLA, sodium selenite and RLA-Se chelates.

transition occurs in $-NH_2$ or –OH owing to the convolution and folding of the peptide chain, which increases the range of the conjugated system, thereby promoting the redshift. And there is no absorption peak in the range of 200–400 nm in sodium selenite solution, which proves that the peptide reacts with selenium. At the same time, compared to the tripeptide RLA, the RLA-Se chelate also had a chromogenic effect at the maximum absorption peak. When the molecular orbital of $-CH_3$ on the side chain group folds with the π system, it has a certain chromogenic effect. A new characteristic absorption peak was observed with RLA-Se near 385 nm, which belongs to the R-band absorption peak, usually caused by the unsaturated group-containing lone electron pair in a p–π conjugate system such as C=O. By comparing the UV spectra of RLA and RLA-Se chelates, it can be seen that the amino and carboxyl groups of RLA are involved in the coordination of the Se ions and have an auxiliary effect on the side-chain $-CH_3$ group, which is the main site of chelation.

3.4.2 SEM. Accurately weighed dried sample powder was adhered to the sample table using conductive double-sided adhesive. After blowing gently with ear ball, ion sputtering was used to spray the gold coating, and the samples were observed and photographed using field emission scanning electron microscopy (Fig. 4). The particle size of RLA was determined to be 5 μm and it showed a flocculent structure. When the microstructure was observed at 10 000×, RLA showed a noticeable cluster bulge, which had a uniform and regular distribution. The electron micrographs of RLA-Se chelates reveal that the particle size of the chelate becomes smaller, about 2 μm, owing to the phenomenon of aggregation. The chelate has a granular structure. Using microscopy, it was found that some particles were attached to the granular cluster structure, imparting it an irregular distribution.

3.4.3 XRD measurements. The diffraction pattern of the material was analyzed using X-ray diffraction, and the composition and structure of the material were obtained. The X-ray diffraction patterns of RLA and RLA-Se chelates are shown in

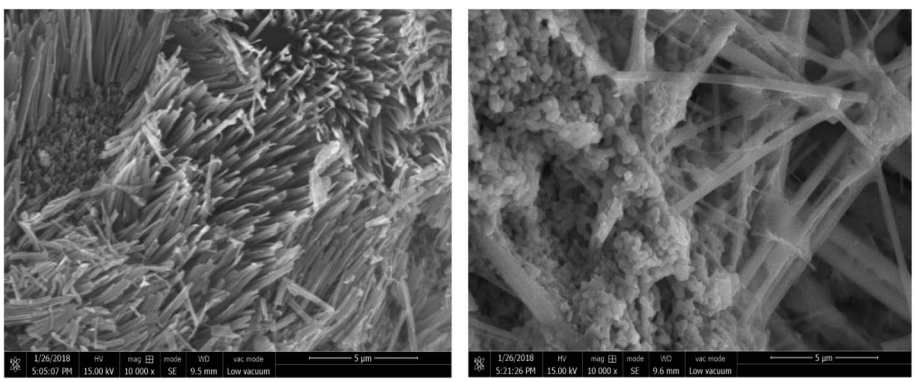

Fig. 4 The SEM images of RLA (left) and RLA-Se (right) chelates.

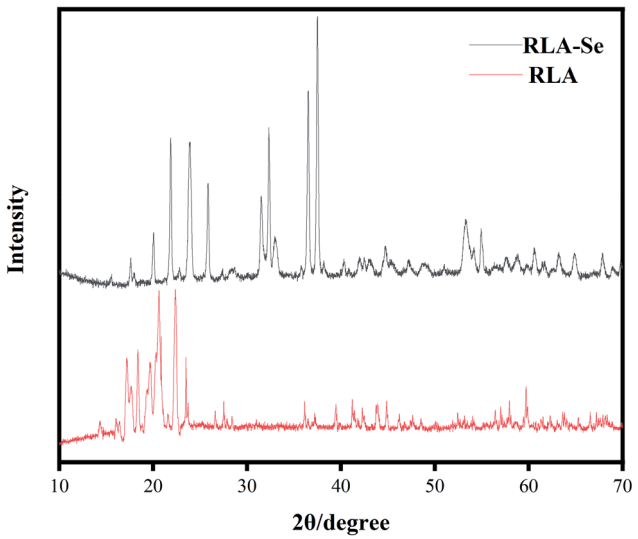

Fig. 5 XRD pattern of RLA and RLA-Se complexes.

Fig. 5. Compared to that of RLA, there were apparent differences in the number, angle, and relative strength of the RLA-Se chelate, indicating the differences in the composition and structure of the chelates. After chelating with selenium ions, the diffraction peaks of most RLA-Se chelates became wider and the particles became smaller, which was consistent with the analytical conclusions derived using SEM. The crystal structure of RLA changed upon the combination of carboxyl, amino, and selenium ions after forming the coordination bond.

3.4.4 ^{1}H-NMR spectroscopy. Fig. 6 shows the ^{1}H-NMR spectrum of the tripeptide, RLA, before and after chelation. It can be seen that compared to that of RLA, the spectra of the RLA-Se chelates showed apparent changes. The chemical shifts of the cleavage peak generated by H spin coupling at different positions of chemical shifts have changed. It is speculated that after chelating with selenium ions, there is a change in the structure of the peptide chain, which affects the chemical environment around H at different positions, resulting in an adjustment of the electron cloud density around the hydrogen nucleus. When the electron cloud density increased, the resonance frequency and the chemical shift both decreased owing to the strong electron shielding effect. The proton signal coupling in RLA was observed at 0.8–0.9 ppm, and the peak of the spectrum showed a split, which indicated that after chelating with the selenium ion, the H of $-CH_3$ on RLA was replaced by a selenium ion to form an ionic bond. These findings were consistent with the results obtained using UV spectroscopy. The peak at 4.2–4.3 ppm increased to 4.5 ppm and almost disappeared. We speculated that $-NH_2$ participated in the chelation reaction, which led to a peak shift to the high field. Similarly, proton coupling also occurred at the position of 1.5–1.6 ppm. The peak split into multiple peaks, and the peak near 1.33 ppm disappeared after chelation. We also speculated that the coordination reaction between the –OH on the carboxyl group and the selenium ion in the chelation process may have caused a change in the spectrum. By comparing the ^{1}H-NMR spectra of RLA and RLA-Se chelates, it was observed that the amino and carboxyl groups of RLA were involved in the coordination of the Se ions and constituted the main sites of chelation. The $-CH_3$ group of R was also involved in the chelation reaction.

3.5 Determination of Se bioavailability using human intestinal Caco-2 cell line

An MTT assay was carried out to determine the cytotoxicity of the RLA-Se chelate and sodium selenite on Caco-2 cells. Both compounds inhibited the proliferation of Caco-2 cells in a dose-dependent manner, and Caco-2 cells were not inactivated at a Se concentration of 8 μM (Fig. 7A). Uptake studies were performed using Caco-2 cells pre-incubated with different concentrations of RLA-Se chelate and cells incubated with sodium Se were used as a control. The change in Se levels in cells was determined using ICP-MS. The Se levels in Caco-2 cells treated with sodium selenite first increased, and then decreased with the additional sodium selenite. The effect of RLA-Se chelate on the absorption of Se in Caco-2 cells increased with an increase in dose. When

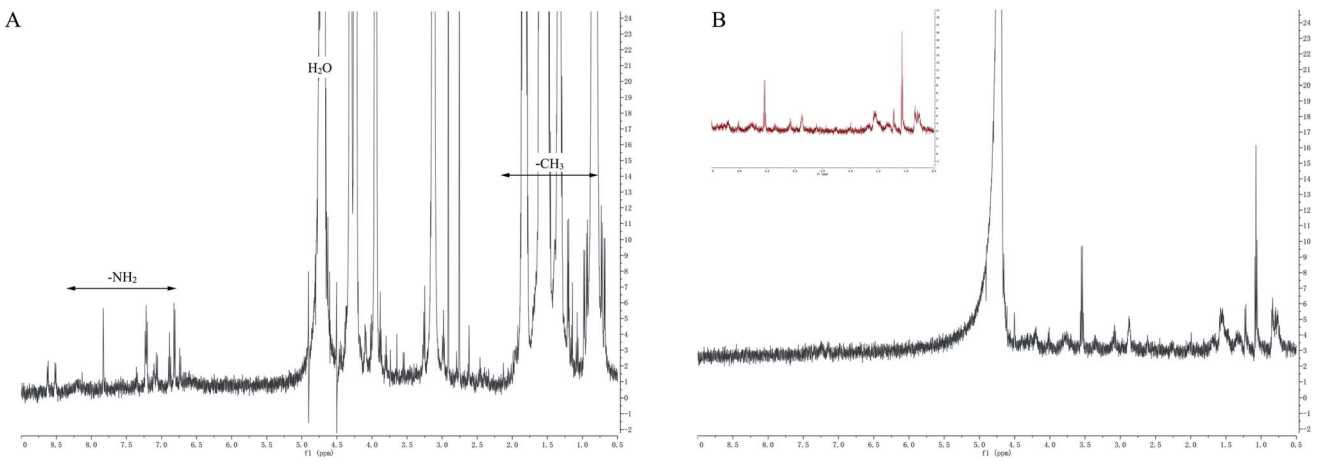

Fig. 6 ^{1}H NMR spectrum of RLA (A) and RLA-Se (B) complexes.

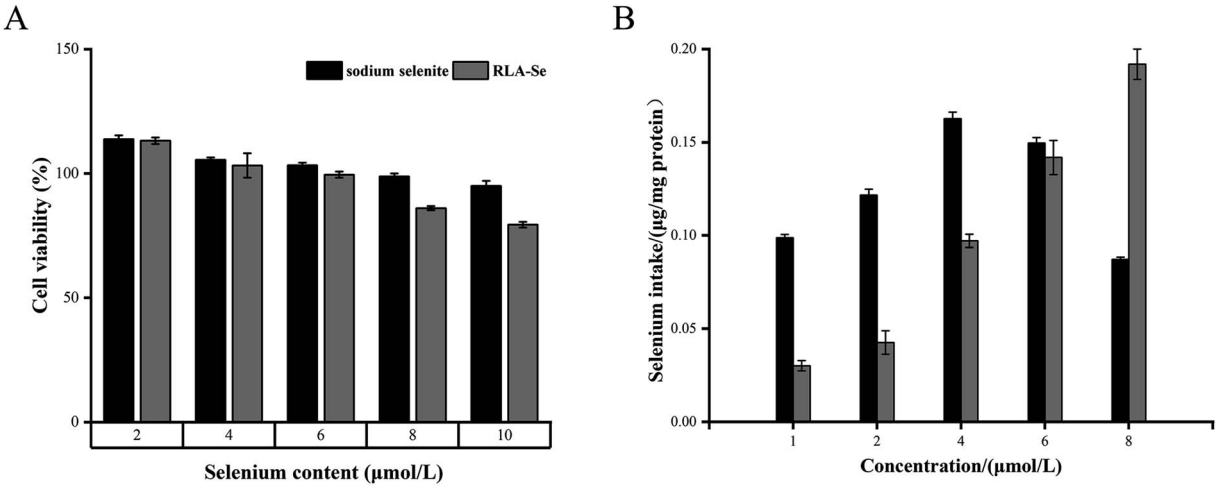

Fig. 7 (A) MTT assay was performed to determine the cytotoxic effect of RLA-Se chelate and sodium selenite. (B) Cellular uptake of RLA-Se chelate and sodium selenite by ICP-MS.

the Se concentration was 8 μM, its levels remained stable (Fig. 7B). At this time, the selenium level in Caco-2 cells was 0.19 μg mg^{-1} protein, which was significantly higher than that of sodium Se ($P < 0.01$).

3.6 Bioinformatics analysis

3.6.1 Identification of differentially expressed proteins. Using iTRAQ-labeled tandem mass spectrometry, 4256 proteins were identified in the control and treated groups (3 replicates in each group). Taking the difference multiple >1.2 or <0.83 as the screening standard of difference protein, the difference protein in the control and treated groups was compared and analyzed, and the upregulated or downregulated protein and the specifically expressed protein in each group was obtained. The results are shown in Table 3.

3.6.2 GO notes. GO functional annotation has a standard definition of a three-level structure, including biological process (BP), molecular function (MF), and cellular component (CC) to which the protein belongs, namely subcellular localization. The GO function of differentially expressed proteins in the control and treated groups were classified as shown in Fig. 8.

3.6.3 Cell differential proteins. In this study, iTRAQ was used to analyze the proteomics of Caco-2 cells. The differential proteins of Caco-2 cells treated with RLA-Se chelate were analyzed. Results showed that compared to the control group, there were 40 different proteins in the treatment group. Only those proteins related to the regulation of the cell cycle and Se are discussed.

4 Discussion

Cai *et al.*[39] and Chen *et al.*[40] have shown that the molecular mass of peptides with mineral-chelating capacity is 294 and 1033 Da. The iron-binding peptides from cottonseed meal have a molecular mass of less than 3 kDa.[41] In this study, three peptides with different molecular weights were identified using ultrafiltration and their chelating capacity was evaluated. Table 1 shows that fraction F1 has the highest Se chelating capacity. The Se-binding capacity of fraction F1 was determined to be 55.61 ± 4.16 mg g^{-1}, which was significantly different from that of the other two fractions and may be attributed to the type and levels of amino acids in the peptide components. Low-molecular-weight peptides have higher activity, whereas the active Se-binding sites in high-molecular-weight peptides cannot be exposed, resulting in a reduction in the chelating rate.[42,43] The results showed that F1 could easily chelate Se. Therefore, F1 and the F1–Se chelates were selected for further studies.

A low-molecular-weight peptide obtained from the plant can easily bind to mineral ions[44] after G-25 column purification, has been reported to have a greater binding capacity and have significant calcium-binding activity.[45,46] Sephadex G-25 gel filtration chromatography was used to separate the F1 fraction, which had the highest Se-binding capacity. Three main fractions were obtained, namely, F11, F12, and F13. Fig. 1 shows the size-dependent portion of the sample. The Se-binding capacity of F12 was determined to be 73.24 ± 1.78 mg g^{-1}, which was different from the other two fractions. Therefore, F12 was chosen for subsequent purification. The eluent corresponding to the active peak of F12 was collected and separated using semi-preparative C18 RP-HPLC. Within 30 min of retention time, 29 components with absorption peaks were obtained by linear gradient elution (Fig. 2A). Due to the separation by RP-HPLC, the substances with weak hydrophobicity (strong polarity) are eluted first.[47] According to the four indexes of peak shape, peak height, peak area and resolution, five peaks (1, 5, 13, 17 and 22) with high resolution and better peak shape were selected for amino acid sequence analysis.[48–50] Five polypeptides from *Grifola frondosa* were identified by LC-ESI/MS sequencing. The five polypeptides were SL, TL, VL, RLA and ML. As previously reported, the antioxidant activity of these peptides is closely related to their molecular weight, AA composition and sequence, and molecular structure. Here, the molecular weight of the peptide is 219–359 Da, which is consistent with the previous results. The specific metal chelating peptide usually

Table 3 List of differentially expressed proteins

Uniprot accession	Name	Peptides	Treated/control fold	*p*-Value
F1T0J3	Interphotoreceptor matrix proteoglycan 2 OS = *Homo sapiens* GN = IMPG2 PE = 2 SV = 1	1241	1.575937	0.002209
A0A024R2K4	Leucine rich repeat (in FLII) interacting protein 2, isoform CRA_b OS = *Homo sapiens* GN = LRRFIP2 PE = 4 SV = 1	742	1.545024	0.001082
Q9BRX9	WD repeat domain-containing protein 83 OS = *Homo sapiens* GN = WDR83 PE = 1 SV = 1	315	1.4814	0.020892
O00257	E3 SUMO-protein ligase CBX4 OS = *Homo sapiens* GN = CBX4 PE = 1 SV = 3	560	1.478102	0.003381
Q13625	Apoptosis-stimulating of p53 protein 2 OS = *Homo sapiens* GN = TP53BP2 PE = 1 SV = 2	1128	1.380386	0.035219
E7EQB3	tRNA-splicing endonuclease subunit Sen34 OS = *Homo sapiens* GN = TSEN34 PE = 1 SV = 2	315	1.371411	0.034023
Q96BW5	Phosphotriesterase-related protein OS = *Homo sapiens* GN = PTER PE = 1 SV = 1	349	1.334326	0.034962
A0A024R7N7	Interferon, gamma-inducible protein 30, isoform CRA_b OS = *Homo sapiens* GN = IFI30 PE = 4 SV = 1	250	1.32053	0.031198
Q5JPC1	Putative uncharacterized protein DKFZp667O1614 OS = *Homo sapiens* GN = DKFZp667O1614 PE = 2 SV = 1	320	1.320405	0.002719
A0A087WXL6	Vacuolar protein sorting 11 (yeast), isoform CRA_a OS = *Homo sapiens* GN = VPS11 PE = 1 SV = 1	941	1.268012	0.031961
O14965	Aurora kinase A OS = *Homo sapiens* GN = AURKA PE = 1 SV = 2	403	1.265934	0.041726
A8K2T7	Receptor protein-tyrosine kinase OS = *Homo sapiens* PE = 2 SV = 1	1210	1.265171	0.019797
A0A024R438	ATG9 autophagy related 9 homolog A (*S. cerevisiae*), isoform CRA_a OS = *Homo sapiens* GN = ATG9A PE = 4 SV = 1	839	1.26087	0.035512
B2RDK3	Oxysterol-binding protein OS = *Homo sapiens* PE = 2 SV = 1	480	1.256281	0.034395
A7YA96	Gamma-glutamyl carboxylase OS = *Homo sapiens* GN = GGCX PE = 2 SV = 1	758	1.254265	0.040682
Q4VCS5	Angiomotin OS = *Homo sapiens* GN = AMOT PE = 1 SV = 1	1084	1.253906	0.00667
Q5JTZ9	Alanine-tRNA ligase, mitochondrial OS = *Homo sapiens* GN = AARS2 PE = 1 SV = 1	985	1.252551	0.0296
Q15642	Cdc42-interacting protein 4 OS = *Homo sapiens* GN = TRIP10 PE = 1 SV = 3	601	1.244809	0.03779
A0A044PY82	Protein LOC113230 OS = *Homo sapiens* GN = LOC113230 PE = 1 SV = 1	361	1.244755	0.042187
Q96CP7	Calfacilitin OS = *Homo sapiens* GN = TLCD1 PE = 2 SV = 1	247	1.236526	0.020604
Q08AI8	Uncharacterized protein C2orf54 OS = *Homo sapiens* GN = C2orf54 PE = 2 SV = 2	447	1.235443	0.008035
Q9P0R6	GSK3-beta interaction protein OS = *Homo sapiens* GN = GSKIP PE = 1 SV = 2	139	1.234663	0.034995
A0A0A0MSV9	Tapasin OS = *Homo sapiens* GN = TAPBP PE = 1 SV = 1	504	1.230369	0.016178
Q969U7	Proteasome assembly chaperone 2 OS = *Homo sapiens* GN = PSMG2 PE = 1 SV = 1	264	1.225194	0.038636
V9GYM8	Rho guanine nucleotide exchange factor 2 OS = *Homo sapiens* GN = ARHGEF2 PE = 1 SV = 1	1031	1.21831	0.045723
Q9P2D8	Protein unc-79 homolog OS = *Homo sapiens* GN = UNC79 PE = 2 SV = 4	2635	1.217964	0.01716
E5KBQ3	TRAF2 OS = *Homo sapiens* GN = TRAF2 PE = 2 SV = 1	501	1.214193	0.014041
P82675	28S ribosomal protein S5, mitochondrial OS = *Homo sapiens* GN = MRPS5 PE = 1 SV = 2	430	1.211803	0.014183
A0A024R880	Cyclin-dependent kinase 9 (CDC2-related kinase), isoform CRA_a OS = *Homo sapiens* GN = CDK9 PE = 3 SV = 1	372	1.211151	0.027363
P29590	Protein PML OS = *Homo sapiens* GN = PML PE = 1 SV = 3	882	1.205636	0.006654
Q8TB72	Pumilio homolog 2 OS = *Homo sapiens* GN = PUM2 PE = 1 SV = 2	1066	1.202853	0.032181
P62875	DNA-directed RNA polymerases I, II, and III subunit RPABC5 OS = *Homo sapiens* GN = POLR2L PE = 1 SV = 1	67	1.200165	0.017111
A0A0U1RR79	Glutamine-tRNA ligase (fragment) OS = *Homo sapiens* GN = QARS PE = 1 SV = 1	75	0.827804	0.036984

Table 3 (*Contd.*)

Uniprot accession	Name	Peptides	Treated/control fold	*p*-Value
H7BXP1	NF-kappa-B inhibitor-interacting Ras-like protein 2 OS = *Homo sapiens* GN = NKIRAS2 PE = 1 SV = 1	229	0.817844	0.031648
B4DSI9	cDNA FLJ56483, highly similar to Eukaryotic translation initiation factor 4 gamma 1 OS = *Homo sapiens* PE = 2 SV = 1	1512	0.8104	0.016782
Q6ZSZ5	Rho guanine nucleotide exchange factor 18 OS = *Homo sapiens* GN = ARHGEF18 PE = 1 SV = 3	1173	0.801527	0.03505
P53801	Pituitary tumor-transforming gene 1 protein-interacting protein OS = *Homo sapiens* GN = PTTG1IP PE = 1 SV = 1	180	0.783099	0.039711
F1D8T1	Hepatocyte nuclear factor 4 4 alpha variant 2 OS = *Homo sapiens* GN = NR2A1 PE = 2 SV = 1	474	0.774468	0.016323
Q8NE01	Metal transporter CNNM3 OS = *Homo sapiens* GN = CNNM3 PE = 1 SV = 1	707	0.764848	0.014595
A0A024R2G1	Cysteine-rich with EGF-like domains 1, isoform CRA_b OS = *Homo sapiens* GN = CRELD1 PE = 4 SV = 1	420	0.753902	0.020377

contains two or more AA residues, and the molecular weight is less than 1500 Da.[51] In addition, hydrophobic and antioxidant AAs, such as Val (V), Leu (L) and Ile (I) can also scavenge free radicals and contribute significantly to antioxidant activity through their interaction with lipids or as strong proton/hydrogen donors.[52,53] In this study, the five peptides contained hydrophobic AA residues and antioxidant AA residues. Usually, high-molecular-weight peptides inhibit the absorption of minerals in the intestine.[54] Therefore, dipeptides and tripeptides are considered suitable options. Leu might have likely played a role in the Se-chelating activity of the five peptides. Moreover, GF is a Leu-rich medicinal mushroom.[55] In peptide no. 4, Arg[56] and Ala[57] are the main amino acids supporting the mineral binding of the purified nonapeptide. In peptide no. 1, the phosphorylation of Ser introduces a negatively charged phosphate group, which serves as a binding site for positively charged metal ions[58] such as those of iron.[59] Additionally, Thr, Val, and Met in peptides 2, 3, and 5 are the related amino acids playing a role in the mineral binding of the purified peptides.[60] In general, according to the reported structure–activity relationship of chelating peptides, the identified peptides seem to have good chelating activity and antioxidant activity. However, further evaluation of synthetic peptides is needed to better study their biological characteristics. The results showed that RLA had the strongest Se-chelating ability with a chelating capacity of 84.47 mg g^{-1} (Fig. 2C). It was speculated that the Arg and Ala residues in the tripeptide and the amino acid residues belonging to the hydrophobic group had more recognition sites and could result in better binding to selenium. It has been demonstrated that the oxygen atom on the carboxyl group of the amino acid residue can form a coordination bond through the electron pair, thereby characterizing the structural characteristics of the purified peptide to create a favorable metal-chelating environment. Therefore, we hypothesized that the carboxylate group of Arg, as well as the imino (NH) and carbonyl (CO) groups in RLA might be involved in the formation of the coordination bond with Se.

To provide additional information about the binding of metal ions to peptide organic ligands, the UV, SEM, XRD, and ^{1}H-NMR spectra are shown. The results from XRD and SEM show an obvious change in the size and the structure of RLA after chelating the selenium ions, which are consistent with the results from previous studies.[61,62] Combined with NMR data, we found that the structure of peptide chain changes after chelating selenium ions, thereby affecting the chemical environment of the H at different positions and changing the electron density surrounding the hydrogen nucleus. In the range of 0.8–0.9 ppm, proton signal-coupling appeared in RLA and the spectral peak showed splitting. These findings indicated that after chelating with selenium ions, the H of $-CH_3$ in RLA was replaced by Se to form an ionic bond. The spatial orientation of the $-CH_3$ group was also changed by rotation, and the internal hydrophobic group was exposed, which resulted in the redistribution of the molecular charge, giving rise to conformation changes and resulting in the formation of a new type of chelate. Moreover, similar to that produced by RLA, the UV spectrum of the RLA-Se chelate also indicated a color enhancement at the maximum absorption peak. When the molecular orbital of $-CH_3$ on the side chain group is folded with the π system, it produces a particular color enhancement effect. In conclusion, the amino and carboxyl groups of RLA are involved in the coordination of the Se ions with the participation of the $-CH_3$ side chains, and constitute the primary chelating sites.

The bioavailability of the RLA-Se chelate in the human colon cancer Caco-2 cells was investigated. An MTT assay was used to determine the effects of the RLA-selenium chelate and sodium selenite in Caco-2 cells. The results showed that both the RLA-Se chelate and sodium selenite inhibited cellular proliferation in a dose-dependent manner, and that the Caco-2 cells were not inactivated at a Se concentration of 8 μM. Compared to sodium selenite, RLA-Se chelates were more efficient in the absorption of selenium in a dose-dependent manner. When the concentration of selenium was 4 μmol L^{-1}, the absorption of sodium selenite reached the peak, and when the concentration was 8

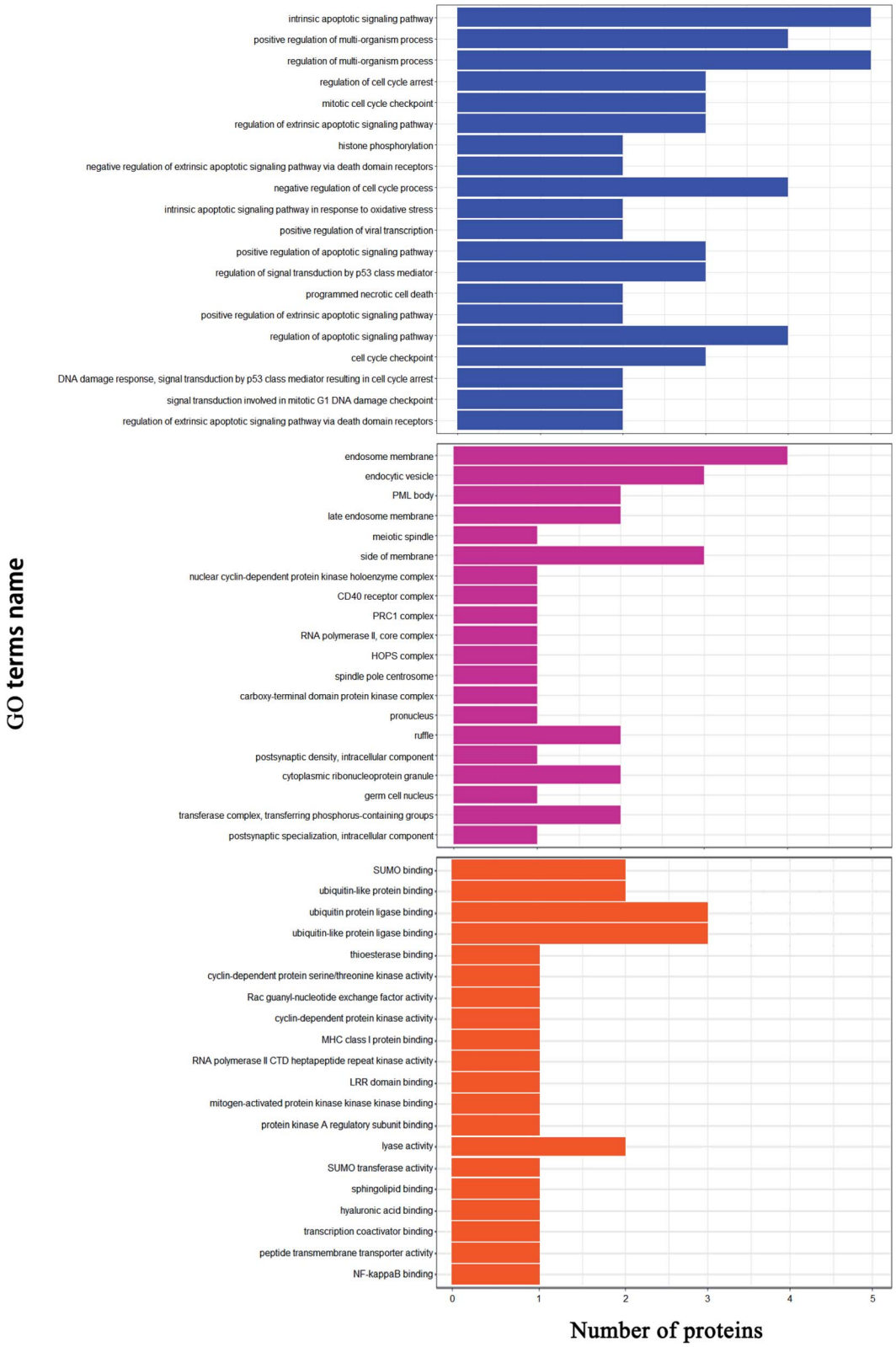

Fig. 8 Gene ontology analysis. Biological processes (blue); cell components (purple); molecular functions (orange).

μmol L^{-1}, the absorption of selenium in sodium selenite decreased sharply, while the absorption of RLA-Se still increased. It shows that when the supplement of selenium is increased, the supplement of inorganic selenium cannot be well absorbed, while RLA-Se can. Numerous studies have shown that organic Se has a better Se-absorption capacity than inorganic

Se.[63] It has been verified that RLA-Se has higher biological activities and lower toxicity compared to sodium selenite. Therefore, the differences in metabolism of RLA-Se warrant further investigation.

In this study, 4256 proteins labeled with quantitative information using iTRAQ were identified. Compared to the healthy control group, there were 40 differentially expressed proteins in the RLA-Se group, among which 22 were significantly upregulated and 8 were significantly downregulated. GO functional annotation, including cell component (CC), biological process (BP), and molecular function (MF), was carried out for the identified differential proteins, to determine the molecular functions and biological processes of proteins that were significantly enriched. The results revealed that for the biological process, differential proteins were mainly involved in the regulation of the apoptotic signaling pathway, regulation of the multi-organism process, and cell-cycle checkpoint among others. In cell composition, these proteins were mainly located in the endosomal membrane and transferase complex. In terms of molecular function, these differential proteins mainly involve SUMO binding, cyclin-dependent protein kinase activity, and NF-kappa B binding.

Se plays a key role in terminal differentiation, cell growth, and development by controlling the cell cycle. Because the "checkpoint" relationship between the occurrence of cancer and G1-S and G2-M transformation in the cell cycle is becoming increasingly prominent and the cell cycle control mechanism has conservative characteristics, the mechanism of Se in controlling the cell cycle is also the embodiment of Se nutrition. It has been shown that Se reduces cell proliferation and growth by blocking the cell cycle and/or promoting apoptosis.[64–66] Se compounds have shown varying chemopreventive effects.[67] Studies indicate that the levels of TP53BP2 (Tumor protein p53 binding protein 2),[68] AURKA (Aurora kinase A),[69] CDK9 (Cyclin-dependent kinase 9),[70] and ARHGEF2 (RHO guanine nucleotide exchange factor 2)[71] were upregulated in the treated group compared to those in the control group, which contributed to the regulation of cell-cycle progression and cell growth *via* their interactions. These findings indicate that the Se-chelating peptide obtained from GF had a positive effect on transcription regulation, cell apoptosis, and aging.

The requirement of Se also depends on its role at the catalytic site of multiple selenoproteins.[72] Glutathione peroxidase (GSH-Px) is a Se-containing enzyme, which plays a crucial role in reproduction, anti-oxidation, muscle function, and tumor prevention. The reduction of hydroperoxide and hydrogen peroxide is catalyzed by GSH-Px through the reduced glutathione.[73] E3 ubiquitin ligases participate in many physiological processes in cells by regulating the ubiquitination of regulatory proteins. All E3 ligases can connect the target protein and specific E2. Ubiquitin-conjugating enzymes (E2) intervene in the ubiquitination and turnover of specific substrates of the ubiquitin-dependent degradation pathway.[74] A conserved core sequence comprising about 150 amino acids from the $-NH_2$ terminus is present in E2 proteins, and the cysteine residue plays an essential role in the formation of the thiol ester bond with the –COOH terminus of ubiquitin.[75] In this study, the expression of E3 proteins in Caco-2 cells treated with Se was higher than that in the control groups. A higher expression of E2 proteins indicated an increase in cysteine levels. Therefore, RLA-Se may accelerate cysteine increase in Caco-2 cells, thereby promoting the expression of E3 proteins.

5 Conclusions

To summarize, we purified a specific tripeptide, RLA, from GFPH, which had strong Se-chelating ability. We also explored the mechanism of RLA in chelating Se ions by analyzing the protein structure. The absorption profiles of the RLA-Se chelates and sodium selenite was studied using Caco-2 cells. The results from our study indicated that GF protein could be used as a promising source for the preparation of Se-binding peptides, and serve as a dietary supplement in selenium-deficient individuals. We also explored the effect of the RLA-Se chelates on cell growth using iTRAQ quantitative proteomics. The results showed that supplementation with peptide-Se chelates could result in the positive regulation of multiple biological processes in cells and might play a specific anticancer role by regulating cell apoptosis. Overall, the purpose of our study was to determine the efficacy of *Grifola frondosa*-selenium chelates as a supplement in food additives and pharmaceutical products.

Conflicts of interest

There are no conflicts to declare.

Acknowledgements

This work was supported by National Natural Science Fon Agriundation of China (no. 31501432), Fujian Provincial School-enterprise Cooperative Major Project (no. 2017N5003), Fujian Agriculture and Forestry University Leader Scholarship Program (no. xjq201608), Special Fund for Science and Technology Innovation of Fujiaculture and Forestry University (cxzx2019139G), Firestone Foundation of Fujian Provincial Hospital (2020HSJJ04), Regional development project of Fujian Provincial Department of Science and Technology (2020N3002).

References

1 J. Avery and P. Hoffmann, *Nutrients*, 2018, **10**, 1203.
2 Y. Shu, M. Wu, S. Yang, Y. Wang and H. Li, *Clin. Nutr.*, 2020, **10**, 3086–3691.
3 M. Kieliszek and S. Błażejak, *Molecules*, 2016, **21**, 609–625.
4 M. Brummer, S. Hayes, K. A. Dawson and L. M. Lawrence, *J. Anim. Sci.*, 2013, **91**, 2158–2168.
5 J. Hu, Q. Zhao, X. Cheng, C. Selomulya, C. Bai, X. Zhu, X. Li and H. Xiong, *Food Chem.*, 2014, **146**, 531–537.
6 H. D. Mistry, F. B. Pipkin, C. W. G. Redman and L. Poston, *Am. J. Obstet. Gynecol.*, 2012, **206**, 21–30.
7 L. Zhang, Y. Gao, H. Feng, N. Zou, K. Wang and D. Sun, *J. Trace Elem. Med. Biol.*, 2019, **56**, 21–30.
8 H. Ying and Y. Zhang, *Biol. Trace Elem. Res.*, 2019, **192**, 38–50.

9 K. Mohsen, M. Chamani, H. Amanlou, A. Nikkhah and A. A. Sadeghi, *Acta Sci., Anim. Sci.*, 2019, **41**, 44392.
10 M. H. G. Berntssen, T. K. Sundal, P. A. Olsvik, H. Amlund, J. D. Rasinger, V. Sele, K. Hamre, M. Hillestad, L. Buttle and R. Ørnsrud, *Aquat. Toxicol.*, 2017, **192**, 116–126.
11 C. Torresfuentes, M. M. Contreras, I. Recio, M. Alaiz and J. Vioque, *Food Chem.*, 2015, **180**, 194–202.
12 H. T. Wu, W. G. Jin, S. G. Sun, X. S. Li, X. H. Duan, Y. Li, Y. T. Yang, J. R. Han and B. W. Zhu, *Eur. Food Res. Technol.*, 2016, **242**, 713–722.
13 G. Huang, Z. Ren and J. Jiang, *Food Bioprocess Technol.*, 2010, **4**, 1527–1532.
14 L. D. L. Hoz, A. N. Ponezi, R. F. Milani, V. S. N. D. Silva, A. S. D. Souza and M. T. Bertoldo-Pacheco, *Food Chem.*, 2014, **142**, 166–169.
15 D. Jin, X. Liu, X. Zheng, X. Wang and J. He, *Food Chem.*, 2016, **204**, 427–436.
16 N. Sun, P. Cui, S. Lin, C. Yu, Y. Tang, Y. Wei, Y. Xiong and H. Wu, *J. Sci. Food Agric.*, 2017, **97**, 4604–4611.
17 B. Liu, Y. Zhuang and L. Sun, *J. Food Sci.*, 2019, **85**, 114–122.
18 H. Hu, S. Wang, X. Zhu, Q. Li, Y. Fan, D. Cheng and B. Li, *Food Chem.*, 2017, **243**, 389–395.
19 N. Xie, J. Huang, B. Li, J. Cheng, Z. Wang, J. Yin and X. Yan, *Food Chem.*, 2014, **173**, 210–217.
20 M. E. Caetano-S, M. T. Bertoldo-P, A. F. Paes-L and F. M. Netto, *Food Res. Int.*, 2015, **71**, 132–139.
21 B. Boh and M. Berovic, *Int. J. Med. Mushrooms*, 2007, **9**, 89–108.
22 E. N. Alonso, M. J. Ferronato, N. A. Gandini, M. E. Fermento, D. J. Obiol, A. López-R, J. Arévalo, M. E. Villegas, M. M. Facchinetti and A. C. Curino, *Nutr. Cancer*, 2017, **69**, 29–43.
23 N. Kodama, Y. Murata and H. Nanba, *J. Med. Food*, 2004, **7**, 141–145.
24 C. Q. Gu, J. W. Li, F. Chao, M. Jin, X. W. Wang and Z. Q. Shen, *Antiviral Res.*, 2007, **75**, 250–257.
25 W. Zhang, Y. Lu, Y. Zhang, Q. Ding, S. Hussain, Q. Wu, W. Pan and Y. Chen, *Int. J. Food Sci. Technol.*, 2016, **51**, 1055–1061.
26 H. Lei, W. Wang, Q. Wang, S. Guo and L. Wu, *Food Agric. Immunol.*, 2013, **24**, 409–418.
27 W. Shen and T. Matsui, *Int. J. Food Sci. Technol.*, 2019, **54**, 1942–1948.
28 I. B. O'Loughlin, P. M. Kelly, B. A. Murray, J. Richard and B. Andre, *J. Agric. Food Chem.*, 2015, **63**, 2708–2714.
29 Z. Zhang, F. Zhou, X. Liu and M. Zhao, *Food Chem.*, 2018, **258**, 269–277.
30 M. V. Chaud, C. Izumi, Z. Nahaal, T. Shuhama, M. L. P. Bianchi and O. Freitaset, *J. Agric. Food Chem.*, 2002, **50**, 871–877.
31 M. J. Dunn and H. J. Kraus, *Proteomics: Clin. Appl.*, 2016, **10**, 1–3.
32 Z. H. Chen, B. Liu and L. N. Zhao, *Food Sci. Technol. Res.*, 2020, **26**, 101–110.
33 P. W. Wesl and C. Cimerman, *Anal. Chem.*, 2002, **36**, 2013–2016.
34 X. Y. Qin, J. T. Zhang, G. M. Li, M. Zhou, R. Z. Gu, J. Lu and W. Y. Liu, *J. Funct. Foods*, 2019, **64**, 103619.
35 F. Hassan, G. A. El-Hiti, M. Abd-Allateef and E. Yousif, *Saudi Med. J.*, 2017, **38**, 359–365.
36 L. Chen, Z. Yu, Y. Lee, X. Wang, B. Zhao and Y. M. Jung, *Analyst*, 2012, **137**, 5834–5838.
37 M. M. Bradford, *Anal. Biochem.*, 1976, **72**, 248–254.
38 J. R. Wiśniewski, A. Zougman, N. Nagaraj and M. Mann, *Nat. Methods*, 2009, **6**, 359–362.
39 X. Cai, Q. Yang, J. Lin, N. Fu and S. Wang, *Molecules*, 2017, **22**, 544.
40 D. Chen, X. Mu, H. Huang, R. Nie, Z. Liu and M. Zeng, *J. Funct. Foods*, 2014, **6**, 575–584.
41 N. H. Kim, S. H. Jung, J. Kim, S. H. Kim, H. J. Ahn and K. B. Song, *J. Korean Soc. Appl. Biol. Chem.*, 2014, **57**, 91–95.
42 X. Wang, A. Gao, Y. Chen, X. Zhang, S. Li and Y. Chen, *Food Chem.*, 2017, **229**, 487–494.
43 H. Tanzadehpanah, A. Asoodeh, M. Saidijam, J. Chamani and H. Mahaki, *J. Biomol. Struct. Dyn.*, 2018, **36**, 3803–3818.
44 L. Zhao, Q. Huang, S. Huang, J. Lin, S. Wang, Y. Huang, J. Hong and P. Rao, *J. Agric. Food Chem.*, 2014a, **62**, 10274–10282.
45 L. Zhao, S. Huang, X. Cai, J. Hong and S. Wang, *J. Funct. Foods*, 2014b, **10**, 46–53.
46 X. Y. Qin, J. T. Zhang, G. M. Li, M. Zhou, R. Z. Gu, J. Lu and W. Y. Liu, *J. Funct. Foods*, 2020, **64**, 103619.
47 G. P. S. Jadaun, S. Dixit, V. Saklani, S. Mendiratta, R. Jain and S. Singh, *Pharm. Methods*, 2016, **8**, 139–144.
48 S. B. Zhang, Z. Wang, S. Y. Xu and X. F. Gao, *J. Am. Oil Chem. Soc.*, 2019, **86**, 959–966.
49 P. Puchalska, M. L. Marina Alegre and M. C. Garcia Lopez, *Crit. Rev. Food Sci. Nutr.*, 2015, **55**, 521–551.
50 A. Sila and A. Bougatef, *J. Funct. Foods*, 2016, **21**, 10–26.
51 B. H. Sarmadi and A. Ismail, *Peptides*, 2010, **31**, 1949–1956.
52 A. G. P. Samaranayaka and C. Li, *J. Funct. Foods*, 2011, **3**, 229–254.
53 G. C. Tenore, A. Ritieni, P. Campiglia, P. Stiuso, S. Di Maro, E. Sommella, G. Pepe, E. D'Urso and E. Novellino, *J. Funct. Foods*, 2015, **15**, 365–375.
54 C. Wang, B. Li and J. Ao, *Food Chem.*, 2012, **134**, 1231–1238.
55 S. J. Huang, S. Y. Tsai, S. Y. Lin, C. H. Liang and J. L. Mau, *Int. J. Med. Mushrooms*, 2011, **13**, 265–272.
56 C. Megías, J. Pedroche, M. M. Yust, J. Girón-Calle, M. Alaiz, F. Millán and J. Vioque, *J. Agric. Food Chem.*, 2007, **55**, 3949–3954.
57 F. R. Liu, L. Wang, R. Wang and Z. X. Chen, *J. Agric. Food Chem.*, 2013, **61**, 7537–7544.
58 E. Miquel and R. Farré, *Trends Food Sci. Technol.*, 2007, **18**, 139–143.
59 R. Palika, P. C. Mashurabad, M. K. Nair, G. B. Reddy and R. Pullakhandam, *Food Res. Int.*, 2014, **67**, 308–314.
60 G. R. Huang, Z. Y. Ren, J. X. Jiang and W. W. Chen, *Adv. J. Food Sci. Technol.*, 2012, **4**, 207–212.
61 B. Mannini, J. Habchi, S. Chia, F. S. Ruggeri, M. Perni, T. P. Knowles, C. M. Dobson and M. Vendruscolo, *ACS Chem. Neurosci.*, 2018, **9**, 2959–2971.

62 Y. G. Jin, W. W. Fu and M. H. Ma, *Afr. J. Biotechnol.*, 2011, **10**, 10204–10211.
63 S. Todd, D. Thomas and W. Hendriks, *J. Anim. Physiol. Anim. Nutr.*, 2012, **96**, 148–158.
64 S. Zhang, X. Peng, J. Fang, H. Cui, Z. Zuo and Z. Chen, *Biol. Trace Elem. Res.*, 2014, **160**, 32–40.
65 H. Zeng, *J. Nutr.*, 2002, **132**, 674–679.
66 H. Zeng and J. H. Botnen, *Biofactors*, 2007, **31**, 55–164.
67 X. Cai, L. Zhao, S. Wang and P. Rao, *Food Funct.*, 2015, **6**, 816–823.
68 Q. Song, J. Song, Q. Wang, Y. Ma, N. Sun, J. Ma, Q. Chen, G. Xia, Y. Huo and L. Yang, *Cancer Med.*, 2016, **5**, 315–324.
69 A. Jacobsen, L. J. Bosch, S. R. Martens-de, B. Carvalho, A. H. Sillars-Hardebol, R. J. Dobson, E. De Rinaldis, G. A. Meijer, S. Abeln and J. Heringa, *Sci. Rep.*, 2018, **8**, 1–11.
70 G. De Falco, L. M. Neri, M. De Falco, C. Bellan, Z. Yu, A. De Luca, L. Leoncini and A. Giordano, *Oncogene*, 2002, **21**, 7464–7470.
71 C. W. Cheon, D. H. Kim, Y. H. Cho and J. H. Kim, *World J. Gastroenterol.*, 2009, **15**, 310.
72 L. Fu, X. Yan, X. Ruan, J. Lin and Y. Wang, *Nanoscale Res. Lett.*, 2014, **9**, 589.
73 Y. Mehdi, J. L. Hornick, L. Istasse and I. Dufrasne, *Molecules*, 2013, **18**, 3292–3311.
74 M. T. Haldeman, G. Xia, E. M. Kasperek and C. M. Pickart, *Biochemistry*, 1997, **36**, 10526–10537.
75 W. J. Cook, L. C. Jeffrey, M. L. Sullivan and R. D. Vierstra, *J. Biol. Chem.*, 1992, **267**, 15116–15121.